

Magnetic interactions in the $S = 1/2$ square-lattice antiferromagnets $\text{Ba}_2\text{CuTeO}_6$ and Ba_2CuWO_6 : parent phases of a possible spin liquid

Otto Mustonen,^{*ab} Sami Vasala,^{cd} Heather Mutch,^b Chris I. Thomas,^a Gavin B. G. Stenning,^e Elisa Baggio-Saitovitch,^c Edmund J. Cussen^b and Maarit Karppinen^{*a}

a. Department of Chemistry and Materials Science, Aalto University, FI-00076 Espoo, Finland. E-mail:

maarit.karppinen@aalto.fi and ohj.mustonen@gmail.com

b. Department of Materials Science and Engineering, University of Sheffield, Mappin Street, Sheffield S1 3JD, United Kingdom.

c. Centro Brasileiro de Pesquisas Físicas (CBPF), Rua Dr Xavier Sigaud 150, Urca, Rio de Janeiro, 22290-180, Brazil.

d. Technische Universität Darmstadt, Institut für Materialwissenschaft, Fachgebiet Materialdesign durch Synthese, Alarich-Weiss-Straße 2, 64287 Darmstadt, Germany

e. ISIS Neutron and Muon Source, Rutherford Appleton Laboratory, Harwell Science and Innovation Campus, Didcot, OX11 0QX, United Kingdom.

The isostructural double perovskites $\text{Ba}_2\text{CuTeO}_6$ and Ba_2CuWO_6 are shown by theory and experiment to be frustrated square-lattice antiferromagnets with opposing dominant magnetic interactions. This is driven by differences in orbital hybridisation of Te^{6+} and W^{6+} . A spin-liquid-like ground state is predicted for $\text{Ba}_2\text{Cu}(\text{Te}_{1-x}\text{W}_x)\text{O}_6$ solid solution similar to recent observations in $\text{Sr}_2\text{Cu}(\text{Te}_{1-x}\text{W}_x)\text{O}_6$.

Magnetic frustration can stabilise novel quantum ground states such as quantum spin liquids or valence bond solids.¹ Frustration occurs when not all of the magnetic interactions in a material can be satisfied simultaneously as a result of lattice geometry or competing interactions. We have recently shown that a quantum-spin-liquid-like state forms in the double perovskite solid solution $\text{Sr}_2\text{Cu}(\text{Te}_{1-x}\text{W}_x)\text{O}_6$ with a square lattice of Cu^{2+} ($3d^9$, $S = 1/2$) cations.^{2,3} This was the first observation of a spin-liquid-like state in a square-lattice compound after 30 years of theoretical predictions.⁴⁻⁷

The parent compounds $\text{Sr}_2\text{CuTeO}_6$ and Sr_2CuWO_6 are frustrated square-lattice (FSL) antiferromagnets.⁸⁻¹² The FSL model (Fig. 1) has two interactions: nearest-neighbour J_1 interaction (side) and next-nearest-neighbour J_2 interaction (diagonal). Dominant antiferromagnetic J_1 leads to Néel type antiferromagnetic order and dominant J_2 leads to columnar magnetic order. Magnetic frustration arises from the competition of J_1 and J_2 , and a quantum spin liquid state has been predicted for $J_2/J_1 = 0.5$ where frustration is maximised.⁴⁻⁷

$\text{Sr}_2\text{CuTeO}_6$ and Sr_2CuWO_6 are the first known isostructural FSL systems with different dominant interactions and magnetic structures: dominant J_1 and Néel order for $\text{Sr}_2\text{CuTeO}_6$ and dominant J_2 and columnar order for Sr_2CuWO_6 respectively.^{8,9} The two compounds have a tetragonal I_4/m double perovskite structure with nearly identical bond distances and angles.^{10,12} The magnetism becomes highly two-dimensional as a result of a Jahn-Teller distortion as the only unoccupied Cu orbital $3d_{x^2-y^2}$ is in the ab square plane. The major differences in dominant magnetic interactions are due to the diamagnetic Te^{6+} d^{10} and W^{6+} d^0 cations located in the middle of the Cu^{2+} square (Fig. 1c), which hybridise differently with O $2p$ allowing different superexchange paths between the Cu^{2+} cations.^{13,14} The spin-liquid-like ground state forms when these two perovskites are

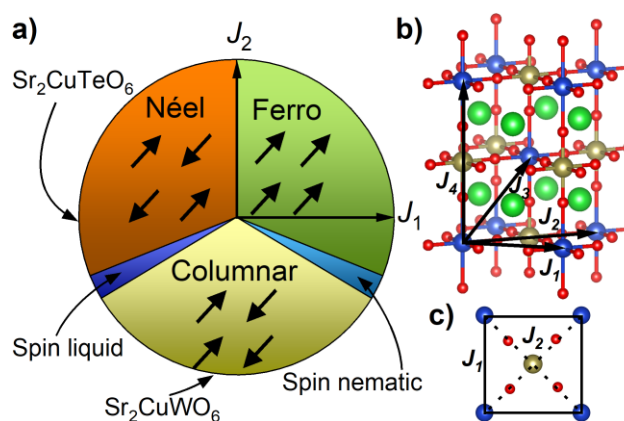


Fig. 1. a) Phase diagram of the frustrated square-lattice model. Antiferromagnetic (negative) J_1 stabilises Néel order and J_2 columnar order respectively. A spin liquid state has been predicted for the Néel-columnar boundary at $J_2/J_1 = 0.5$ where magnetic frustration is maximised. b) The double perovskite structure of $(\text{Ba,Sr})_2\text{Cu}(\text{Te,W})\text{O}_6$. J_1 and J_2 are the in-plane interactions of the FSL model, whereas J_3 and J_4 are out-of-plane interactions. The blue, dark yellow, red and green spheres represent Cu, Te/W, O and Ba/Sr, respectively. c) The Cu^{2+} square in the ab plane with J_1 and J_2 interactions.

mixed into a $\text{Sr}_2\text{Cu}(\text{Te}_{1-x}\text{W}_x)\text{O}_6$ solid solution.^{2,3,15} Muon spin relaxation experiments revealed the absence of magnetic order or static magnetism in a wide composition range of $x = 0.1-0.6$.^{2,3} The specific heat displays T -linear behaviour suggesting gapless excitations in a similar composition range.^{2,3,15} The ground state has been proposed to be a random-singlet state with a disordered arrangement of non-magnetic valence bond singlets.¹⁶

Motivated by these exciting findings in the $\text{Sr}_2\text{Cu}(\text{Te}_{1-x}\text{W}_x)\text{O}_6$ system, we have investigated the magnetic interactions of the isostructural barium analogues $\text{Ba}_2\text{CuTeO}_6$ and Ba_2CuWO_6 . Ba_2CuWO_6 is known to have columnar magnetic order,^{17,18} but little is known about $\text{Ba}_2\text{CuTeO}_6$ as the perovskite phase requires high pressures to synthesise.¹⁹ Here we use density functional theory (DFT) calculations and high-temperature series expansion (HTSE) fitting of experimental susceptibility data to show that these compounds are FSL antiferromagnets with opposite dominant interactions similar to $\text{Sr}_2\text{CuTeO}_6$ and Sr_2CuWO_6 . We predict a quantum-spin-liquid-like

state in $\text{Ba}_2\text{Cu}(\text{Te}_{1-x}\text{W}_x)\text{O}_6$ with strong antiferromagnetic interactions.

Magnetic interactions and electronic structure in $\text{Ba}_2\text{CuTeO}_6$ and Ba_2CuWO_6 were calculated using the DFT+ U framework, where an on-site Coulomb repulsion term U was used to model electron correlation effects of localised Cu $3d$ orbitals. Interactions up to the fourth-nearest neighbour were evaluated, see Fig. 1b. J_1 and J_2 are the square plane interactions of the FSL model, and J_3 and J_4 are additional out-of-plane interactions. Energies of different spin configurations were mapped onto a Heisenberg Hamiltonian to obtain J_1 - J_4 . We have previously shown this approach works well for Sr_2CuWO_6 .⁹ The J_1 and J_2 interactions were also determined from experimental magnetic susceptibility data using high-temperature series expansion fitting. $\text{Ba}_2\text{CuTeO}_6$ was prepared by high-pressure synthesis and Ba_2CuWO_6 by conventional solid state synthesis. Details of the DFT calculations, sample synthesis and characterisation are available in the electronic supporting information (ESI).

Table 1. Exchange constants of $\text{Ba}_2\text{CuTeO}_6$ and Ba_2CuWO_6 obtained by density functional theory using different on-site Coulomb U terms and by high-temperature series expansion fitting of magnetic susceptibility data. Negative (positive) values correspond to antiferromagnetic (ferromagnetic) interactions.

$\text{Ba}_2\text{CuTeO}_6$	$U = 7$ eV	$U = 8$ eV	$U = 9$ eV	HTSE
J_1 (meV)	-23.65	-20.22	-17.22	-16.54(3)
J_2 (meV)	0.13	0.23	0.06	-0.04(3)
J_3 (meV)	1.28	0.83	0.67	-
J_4 (meV)	-0.30	0.01	0.05	-
J_2/J_1	-0.01	-0.01	-0.003	0.002
Ba_2CuWO_6	$U = 7$ eV	$U = 8$ eV	$U = 9$ eV	HTSE
J_1 (meV)	-1.25	-1.17	-1.27	0.2(9)
J_2 (meV)	-14.71	-11.94	-9.56	-10.0(1)
J_3 (meV)	0.05	-0.01	0.01	-
J_4 (meV)	0.03	0.37	0.02	-
J_2/J_1	11.79	10.18	7.55	-50*

*significant uncertainty in this value due to error in J_1

The calculated magnetic interactions of $\text{Ba}_2\text{CuTeO}_6$ and Ba_2CuWO_6 are presented in Table 1. The calculated values depend on the Coulomb U term as is typical with DFT+ U , but the same trends are observed for reasonable values of U . Despite being isostructural, the magnetic interactions in $\text{Ba}_2\text{CuTeO}_6$ and Ba_2CuWO_6 are very different. $\text{Ba}_2\text{CuTeO}_6$ has a very dominant antiferromagnetic J_1 interaction with weak J_2 , J_3 and J_4 interactions. It is a near-ideal FSL Néel antiferromagnet. Ba_2CuWO_6 , in contrast, has a dominant antiferromagnetic J_2 interaction slightly frustrated by an antiferromagnetic J_1 interaction with negligible J_3 and J_4 interactions. The strong J_2 interaction is consistent with the known columnar magnetic structure of this compound.¹⁸ Due to the weakness of the out-of-plane J_3 and J_4 interactions, magnetism in both compounds is highly two-dimensional and well described by the FSL model.

The significant differences in the magnetic interactions of $\text{Ba}_2\text{CuTeO}_6$ and Ba_2CuWO_6 can be explained by their electronic structures. We have plotted total and partial densities of states

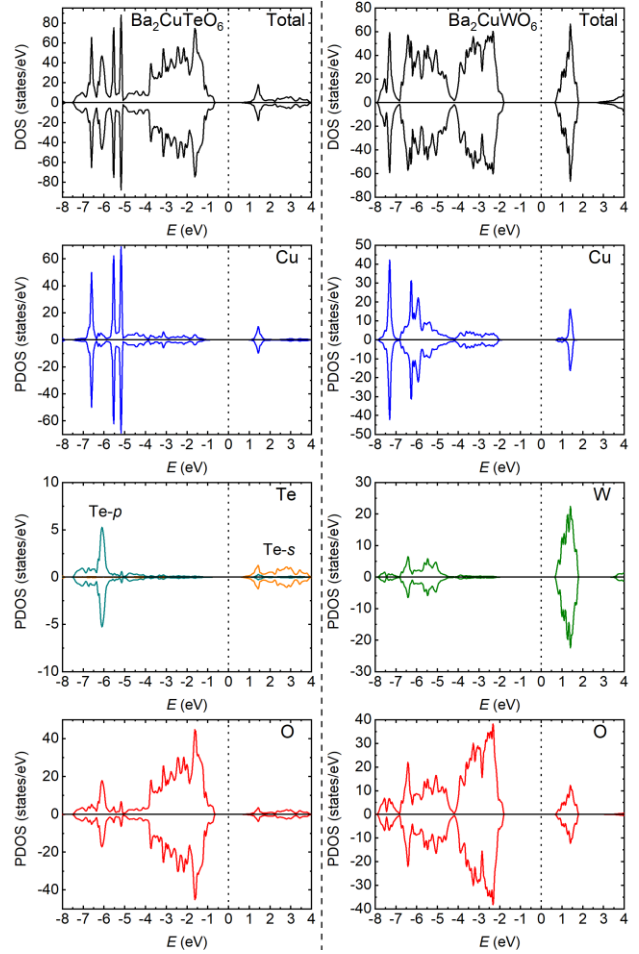


Fig. 2. Total and partial density of states plots for $\text{Ba}_2\text{CuTeO}_6$ (left) and Ba_2CuWO_6 (right). Both compounds are antiferromagnetic insulators. The moderate Te $5p/5s - O 2p$ hybridisation and stronger W $5d - O2p$ hybridisation are seen in the Te/W and O PDOS plots.

for both compounds in Fig. 2. $\text{Ba}_2\text{CuTeO}_6$ and Ba_2CuWO_6 are antiferromagnetic insulators: the band gaps open between the occupied Cu $3d$ states hybridised with O $2p$ (valence band) and the unoccupied Cu $3d_{x^2-y^2}$ states hybridised with O $2p$ (conduction band). In Ba_2CuWO_6 the conduction band is further hybridised with unoccupied W $5d$ states. The W $5d$ states also hybridise with the Cu $3d/O 2p$ states in the valence band, which allows a 180° Cu-O-W-O-Cu superexchange pathway resulting in a strong antiferromagnetic J_2 interaction. This hybridisation does not occur in $\text{Ba}_2\text{CuTeO}_6$ and therefore J_2 is negligible. In $\text{Ba}_2\text{CuTeO}_6$ the Te $5p$ states hybridise to a lesser degree with the Cu $3d/O 2p$ states in the conduction band, which could explain the strong antiferromagnetic J_1 interaction. However, the role of Te in the J_1 superexchange in $\text{Sr}_2\text{CuTeO}_6$ is under debate.^{8,13} Overall, the electronic structures of $\text{Ba}_2\text{CuTeO}_6$ and Ba_2CuWO_6 are similar to their strontium analogues $\text{Sr}_2\text{CuTeO}_6$ and Sr_2CuWO_6 , and the differences in magnetic interactions are driven by the same orbital hybridisation mechanism.

The experimental magnetic susceptibilities of synthesised $\text{Ba}_2\text{CuTeO}_6$ and Ba_2CuWO_6 samples are shown in Fig. 3. The broad maximum observed in the susceptibility is due to the two-dimensional nature of the magnetism in these materials. Our maximum temperature of 400 K was not enough for reliable

Curie-Weiss fits. Previous measurements¹⁹ up to 800 K yielded the Curie-Weiss constants $\Theta_{CW} = -400$ K for $\text{Ba}_2\text{CuTeO}_6$ and $\Theta_{CW} = -249$ K for Ba_2CuWO_6 revealing strong antiferromagnetic interactions.

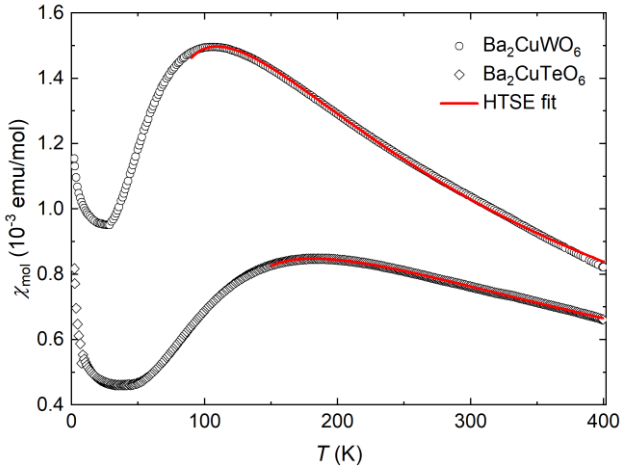


Fig. 3. Magnetic susceptibility and high-temperature series expansion fits for $\text{Ba}_2\text{CuTeO}_6$ and Ba_2CuWO_6 . Open symbols represent experimental data and the lines are HTSE fits with the parameters $J_1 = -16.54(3)$ meV, $J_2 = -0.04(3)$ meV, $g = 2.20(1)$ and $J_1 = 0.2(9)$ meV, $J_2 = -10.0(1)$ meV, $g = 2.26(5)$ for $\text{Ba}_2\text{CuTeO}_6$ and Ba_2CuWO_6 , respectively. The ZFC and FC curves overlap and therefore only ZFC data is shown.

The magnetic susceptibilities were fitted to a high-temperature series expansion of the FSL model.²⁰ The molar magnetic susceptibility χ_{mol} is given by:

$$\chi_{\text{mol}} = \frac{N_A g^2 \mu_B^2}{k_B T} \sum_n \beta^n \sum_m c_{m,n} x^m + \chi_0 \quad (1)$$

where g is the effective g -factor, $\beta = -J_1/k_B$, $x = J_2/J_1$, χ_0 is a temperature independent diamagnetic correction and the coefficients $c_{m,n}$ are from Table I in ref. 20. The model has four parameters: J_1 , J_2 , g and χ_0 , which were fitted to the experimental data using a least squares method. The model always produces two solutions due to internal symmetry: one with dominant J_1 and one with dominant J_2 .²¹ Our DFT calculations allow us to select the correct dominant J_1 solution for $\text{Ba}_2\text{CuTeO}_6$ and the dominant J_2 solution for Ba_2CuWO_6 .

The best fits were obtained with the parameters $J_1 = 16.54(3)$ meV, $J_2 = -0.04(3)$ meV, $g = 2.20(1)$ for $\text{Ba}_2\text{CuTeO}_6$ and $J_1 = 0.2(9)$ meV, $J_2 = -10.0(1)$ meV, $g = 2.26(5)$ for Ba_2CuWO_6 in the temperature ranges 150-400 K and 90-400 K, respectively. The fitted exchange constants depend slightly on the minimum temperature used. For both compounds the calculated dominant interaction remains stable in a wide fitting range, but the weaker interaction cannot be accurately quantified. In $\text{Ba}_2\text{CuTeO}_6$ the sign of J_2 changes depending on the fitting range, whereas in Ba_2CuWO_6 the error of J_1 is much larger than its value. We can conclude, however, that the dominant interaction is much stronger than the weak one in both $\text{Ba}_2\text{CuTeO}_6$ ($|J_2|/|J_1| < 0.02$) and Ba_2CuWO_6 ($|J_1|/|J_2| < 0.12$) and that the DFT and HTSE results are in good agreement.

The magnetic properties of $\text{Ba}_2\text{CuTeO}_6$, Ba_2CuWO_6 , $\text{Sr}_2\text{CuTeO}_6$ and Sr_2CuWO_6 are summarised in Table 2. Magnetic interactions in $\text{Ba}_2\text{CuTeO}_6$ and Ba_2CuWO_6 are notably stronger than their strontium analogues. This is due to the smaller tilting

of the CuO_6 octahedra in the barium phases, which leads to stronger orbital overlap as the Cu-O-Te/W angle is closer to 180 degrees.¹⁹ As long-range magnetic order is driven by the weak out-of-plane interactions which are of the same order in all compounds, $\text{Ba}_2\text{CuTeO}_6$ and Ba_2CuWO_6 are even closer to ideal two-dimensional antiferromagnets than their strontium analogues. The transition temperature of $\text{Ba}_2\text{CuTeO}_6$ is not known, but we predict it to have the highest frustration index $f = \Theta_{CW}/T_N$ of these compounds and the Néel magnetic structure due to the very strong J_1 interaction. Magnetic excitations in $\text{Sr}_2\text{CuTeO}_6$ and Sr_2CuWO_6 have been observed at temperatures higher than $2T_N$ driven by the two-dimensional magnetic interactions.^{8,9} The stronger in-plane J_1 and J_2 interactions of the barium phases indicate the excitations survive to even higher temperatures.

Table 2. Magnetic properties of $\text{Ba}_2\text{CuTeO}_6$, $\text{Sr}_2\text{CuTeO}_6$, Ba_2CuWO_6 and Sr_2CuWO_6 . Exchange interactions J_1 and J_2 have been obtained by density functional theory (DFT; $U = 8$ eV), high-temperature series expansion fitting (HTSE) or by inelastic neutron scattering (INS). The data for $\text{Ba}_2\text{CuTeO}_6$ and Ba_2CuWO_6 are from this work unless specified otherwise.

	$\text{Ba}_2\text{CuTeO}_6$	$\text{Sr}_2\text{CuTeO}_6$	Ba_2CuWO_6	Sr_2CuWO_6
J_1 (meV)	-20.22 (DFT) -16.54(3) (HTSE)	-7.18 (INS) ⁸	-1.17 (DFT) -0.2(9) (HTSE)	-2.45 (DFT) ⁹ -1.2 (INS) ⁹
J_2 (meV)	0.23 (DFT) -0.04(3) (HTSE)	-0.21 (INS) ⁸	-11.94 (DFT) -10.0(1) (HTSE)	-8.83 (DFT) ⁹ -9.5 (INS) ⁹
Θ_{CW} (K)	-400 ¹⁹	-80 ²	-249 ¹⁹	-165 ²
T_N (K)	-	29 ¹⁰	28 ¹⁸	24 ¹²
$f = \Theta_{CW}/T_N$	-	2.8	8.9	6.9
k	[1/2 1/2 k_z]*	[1/2 1/2 0] ¹⁰	[0 1/2 1/2] ¹⁸	[0 1/2 1/2] ¹¹
Magnetic order	Néel*	Néel	Columnar	Columnar

*predicted based on magnetic interactions

Since $\text{Ba}_2\text{CuTeO}_6$ has a dominant J_1 interaction and Ba_2CuWO_6 has a dominant J_2 interaction, we predict a spin-liquid-like state will form in the $\text{Ba}_2\text{Cu}(\text{Te}_{1-x}\text{W}_x)\text{O}_6$ solid solution similar to $\text{Sr}_2\text{Cu}(\text{Te}_{1-x}\text{W}_x)\text{O}_6$. In the $\text{Sr}_2\text{Cu}(\text{Te}_{1-x}\text{W}_x)\text{O}_6$ system the Néel order is destabilised already at $x = 0.1$, and spin-liquid-like state exist in the composition region $x = 0.1-0.6$. Columnar order is observed for $x = 0.7-1$. Since the J_1 interaction of $\text{Ba}_2\text{CuTeO}_6$ is so strong even compared to J_2 in Ba_2CuWO_6 , we predict the Néel order remains more stable against W substitution. For the same reason, the columnar order near $x = 1$ is likely to be less stable in $\text{Ba}_2\text{Cu}(\text{Te}_{1-x}\text{W}_x)\text{O}_6$. The extent of the spin-liquid-like region depends also on disorder, and is difficult to predict just from the properties of the end phases. Finally, the stronger antiferromagnetic interactions in the barium phases indicate that the quantum disordered ground state will remain stable up to higher temperatures.

The previous discussion concerns a double perovskite $\text{Ba}_2\text{Cu}(\text{Te}_{1-x}\text{W}_x)\text{O}_6$ solid solution, which near $x = 0$ will require high-

pressure synthesis to form. The ambient pressure form of $\text{Ba}_2\text{CuTeO}_6$ is triclinic with a tolerance factor higher than 1.03.²² Therefore, a $\text{Ba}_2\text{Cu}(\text{Te}_{1-x}\text{W}_x)\text{O}_6$ solid solution prepared in ambient pressure will have a triclinic to tetragonal structural change at some composition. Triclinic $\text{Ba}_2\text{CuTeO}_6$ is a spin ladder system close to a quantum critical point,²³ and we propose Te-for-W substitution could drive the system from magnetic order to a spin singlet state.

In conclusion, we have investigated the magnetic interactions of the tetragonal double perovskites $\text{Ba}_2\text{CuTeO}_6$ and Ba_2CuWO_6 by DFT calculations and by HTSE fitting. Both compounds are well described by the frustrated square-lattice model as out-of-plane interactions are very weak. In $\text{Ba}_2\text{CuTeO}_6$ the antiferromagnetic nearest-neighbor J_1 interaction dominates ($|J_2|/|J_1| < 0.02$), whereas in Ba_2CuWO_6 the antiferromagnetic next-nearest neighbor interaction J_2 dominates ($|J_1|/|J_2| < 0.12$). The $\text{Ba}_2\text{Cu}(\text{Te,W})\text{O}_6$ system is the second known FSL system where isostructural compounds have opposite magnetic interactions. This is driven by differences in orbital hybridisation of Te $5p/5s$ and W $5d$ with O $2p$. A spin-liquid-like ground state is predicted for the $\text{Ba}_2\text{Cu}(\text{Te}_{1-x}\text{W}_x)\text{O}_6$ solid solution similar to the recent findings in the $\text{Sr}_2\text{Cu}(\text{Te}_{1-x}\text{W}_x)\text{O}_6$ system.

The authors wish to acknowledge CSC – IT Center for Science, Finland, for computational resources. The authors are thankful for access to the MPMS3 instrument in the Materials Characterisation Laboratory at the ISIS Muon and Neutron Source. OM, HM and EJC are thankful for funding by the Leverhulme Trust Research Project Grant 2017-109. SV is thankful for the support of the Brazilian funding agencies CNPq (grants no. 150503/2016-4 and 152331/2016-6) and FAPERJ (grant no. 202842/2016). EBS is grateful for financial support by a joint DFG-FAPERJ project DFG Li- 244/12. In addition, EBS acknowledges support from FAPERJ through several grants including Emeritus Professor fellow and CNPq for BPA and corresponding grants.

Conflicts of interest

There are no conflicts to declare.

Notes and references

1. L. Balents, *Nature*, 2010, 464, 199–208.
2. O. Mustonen, S. Vasala, E. Sadrollahi, K. P. Schmidt, C. Baines, H. C. Walker, I. Terasaki, F. J. Litterst, E. Baggio-Saitovitch and M. Karppinen, *Nat. Commun.*, 2018, 9, 1085.
3. O. Mustonen, S. Vasala, K. P. Schmidt, E. Sadrollahi, H. C. Walker, I. Terasaki, F. J. Litterst, E. Baggio-Saitovitch and M. Karppinen, *Phys. Rev. B*, 2018, 98, 064411.
4. P. W. Anderson, *Science*, 1987, 235, 1196–1198.
5. F. Mezzacapo, *Phys. Rev. B*, 2012, 86, 045115.
6. H.-C. Jiang, H. Yao and L. Balents, *Phys. Rev. B*, 2012, 86, 024424.
7. W.-J. Hu, F. Becca, A. Parola and S. Sorella, *Phys. Rev. B*, 2013, 88, 060402.
8. P. Babkevich, V. M. Katukuri, B. Fåk, S. Rols, T. Fennell, D. Pajić, H. Tanaka, T. Pardini, R. R. P. Singh, A. Mitrushchenkov, O. V. Yazyev and H. M. Rønnow, *Phys. Rev. Lett.*, 2016, 117, 237203.
9. H. C. Walker, O. Mustonen, S. Vasala, D. J. Voneshen, M. D. Le, D. T. Adroja and M. Karppinen, *Phys. Rev. B*, 2016, 94, 064411.
10. T. Koga, N. Kurita, M. Avdeev, S. Danilkin, T. J. Sato and H. Tanaka, *Phys. Rev. B*, 2016, 93, 054426.
11. S. Vasala, M. Avdeev, S. Danilkin, O. Chmaissem and M. Karppinen, *J. Phys. Condens. Matter*, 2014, 26, 496001.
12. S. Vasala, H. Saadaoui, E. Morenzoni, O. Chmaissem, T. Chan, J. Chen, Y. Hsu, H. Yamauchi and M. Karppinen, *Phys. Rev. B*, 2014, 89, 134419.
13. Y. Xu, S. Liu, N. Qu, Y. Cui, Q. Gao, R. Chen, J. Wang, F. Gao and X. Hao, *J. Phys. Condens. Matter*, 2017, 29, 105801.
14. M. Zhu, D. Do, C. R. Dela Cruz, Z. Dun, H. D. Zhou, S. D. Mahanti and X. Ke, *Phys. Rev. Lett.*, 2014, 113, 076406.
15. M. Watanabe, N. Kurita, H. Tanaka, W. Ueno, K. Matsui and T. Goto, *Phys. Rev. B*, 2018, 98, 054422.
16. K. Uematsu and H. Kawamura, *Phys. Rev. B*, 2018, 98, 134427.
17. Y. Todate, *J. Phys. Soc. Japan*, 2001, 70, 337.
18. Y. Todate, W. Higemoto, K. Nishiyama and K. Hirota, *J. Phys. Chem. Solids*, 2007, 68, 2107–2110.
19. D. Iwanaga, Y. Inaguma and M. Itoh, *J. Solid State Chem.*, 1999, 147, 291–295.
20. H. Rosner, R. R. P. Singh, W. H. Zheng, J. Oitmaa and W. E. Pickett, *Phys. Rev. B*, 2003, 67, 014416.
21. A. A. Tsirlin, R. Nath, A. M. Abakumov, Y. Furukawa, D. C. Johnston, M. Hemmida, H. A. Krug Von Nidda, A. Loidl, C. Geibel and H. Rosner, *Phys. Rev. B*, 2011, 84, 014429.
22. G. N. Rao, R. Sankar, A. Singh, I. P. Muthuselvam, W. T. Chen, V. N. Singh, G.-Y. Guo and F. C. Chou, *Phys. Rev. B*, 2016, 93, 104401.
23. D. Macdougall, A. S. Gibbs, T. Ying, S. Wessel, H. C. Walker, D. Voneshen, F. Mila, H. Takagi and R. Coldea, *Phys. Rev. B*, 2018, 98, 174410.

Magnetic interactions in the $S = 1/2$ square-lattice antiferromagnets $\text{Ba}_2\text{CuTeO}_6$ and Ba_2CuWO_6

Otto Mustonen,^{ab} Sami Vasala,^{cd} Heather Mutch,^b Chris I. Thomas,^a Gavin B. G. Stenning,^e Elisa Baggio-Saitovitch,^c Edmund J. Cussen^b and Maarit Karppinen^{*a}

Electronic Supporting Information

Density functional theory calculations

Density functional theory was used to calculate the magnetic exchange constants in $\text{Ba}_2\text{CuTeO}_6$ and Ba_2CuWO_6 . The calculations were carried out with the full potential linearized augmented plane wave code ELK.¹ We used the generalized gradient approximation functionals by Perdew, Burke and Ernzerhof.² Five different spin configurations with $2 \times 2 \times 1$ ($1 \times 1 \times 2$) supercells were needed to calculate the exchange constants (Fig. 1).^{3,4} A k point grid of $4 \times 4 \times 6$ ($8 \times 8 \times 3$) was used. A plane-wave cutoff of $|G + k|_{\text{max}} = 8/R_{\text{MT}}$ a.u.⁻¹ was used, where R_{MT} was the average muffin tin radius. Electron correlation effects of the localized Cu^{2+} $3d$ orbitals were included within the DFT+ U framework with the on-site coulombic repulsion U and Hund exchange term I as parameters.⁵ The on-site coulombic U term was varied from 7 to 9 eV, which are typical values for Cu $3d$ orbitals. The Hund term I was fixed at 0.9 eV for all calculations.

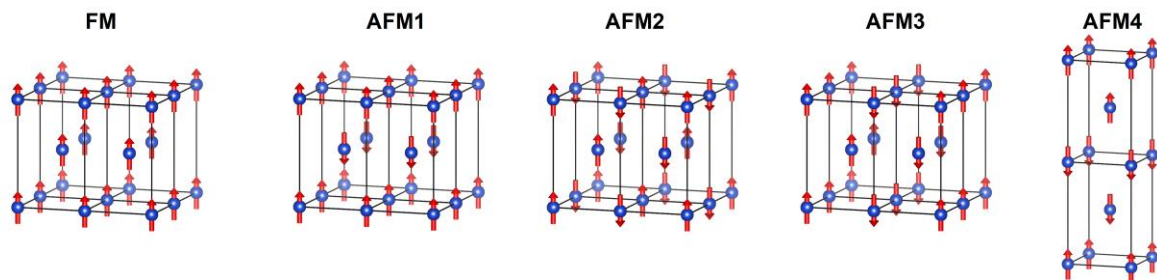


Fig. 1. The five different spin configurations used in the density functional theory calculations. Only the magnetic Cu^{2+} cations and their spins are shown. The energies are calculated in $2 \times 2 \times 1$ (and one $1 \times 1 \times 2$) supercells.

In order to obtain the exchange constants J_1 - J_4 we mapped the energies of the different spin configurations to a simple Heisenberg Hamiltonian:

$$H = - \sum_{i < j} J_{ij} S_i \cdot S_j$$

where J_{ij} is the exchange constant for the interaction between spins i and j . The spin configurations are presented in Fig. 1. Using the Hamiltonian, the energies of the spin configurations³ can be written as:

$$E_{FM} = E_0 + (-4J_1 - 4J_2 - 8J_3 - 2J_4)S^2$$

$$E_{AFM1} = E_0 + (-4J_1 - 4J_2 + 8J_3 - 2J_4)S^2$$

$$E_{AFM2} = E_0 + (4J_1 - 4J_2 - 2J_4)S^2$$

$$E_{AFM3} = E_0 + (4J_2 - 2J_4)S^2$$

$$E_{AFM4} = E_0 + (-4J_1 - 4J_2 + 2J_4)S^2$$

The exchange constants J_1 - J_4 can then be obtained from:³

$$J_3 = (E_{AFM1} - E_{FM})/16S^2$$

$$J_1 = (E_{AFM2} - E_{FM} - 8J_3S^2)/8S^2$$

$$J_2 = (E_{AFM3} - E_{FM} - 4J_1S^2 - 8J_3S^2)/8S^2$$

$$J_4 = (E_{AFM4} - E_{FM} - 8J_3S^2)/4S^2$$

The calculated energies and exchange constants for $U = 7$ - 9 eV are presented in Table 1.

Table 1. Relative total energies of the different spin configurations of Ba_2CuTeO_6 and Ba_2CuWO_6 calculated by density functional theory. Energy of the ferromagnetic configuration is set as zero.

	Ba₂CuTeO₆			Ba₂CuWO₆		
	$U = 7$ eV	$U = 8$ eV	$U = 9$ eV	$U = 7$ eV	$U = 8$ eV	$U = 9$ eV
E_{FM} (meV/2f.u.)	0	0	0	0	0	0
E_{AFM1} (meV/2f.u.)	5.12	3.33	2.67	0.22	-0.04	0.04
E_{AFM2} (meV/2f.u.)	-44.74	-38.78	-33.11	-2.39	-2.37	-2.51
E_{AFM3} (meV/2f.u.)	-20.82	-18.10	-15.77	-30.56	-25.08	-20.36
E_{AFM4} (meV/2f.u.)	2.26	1.67	1.39	0.14	0.35	0.04
J_1 (meV)	-23.65	-20.22	-17.22	-1.25	-1.17	-1.27
J_2 (meV)	0.13	0.23	0.06	-14.71	-11.94	-9.56
J_3 (meV)	1.28	0.83	0.67	0.05	-0.01	0.01
J_4 (meV)	-0.30	0.01	0.05	0.03	0.37	0.02
J_2/J_1	-0.01	-0.01	0.00	11.79	10.18	7.55

Sample synthesis

Ba_2CuWO_6 and triclinic Ba_2CuTeO_6 were prepared using a conventional solid state reaction method from stoichiometric amounts of $BaCO_3$, CuO , WO_3 and TeO_2 (Alpha Aesar ≥ 99.995). The samples were calcined at 900 °C in air for 12 hours, reground, pelletized and fired **twice** at 1000 °C in air for 24 hours. Tetragonal double perovskite Ba_2CuTeO_6 was prepared from triclinic Ba_2CuTeO_6 under high-pressure high-temperature conditions. Sample powder enclosed in a gold capsule was pressed in a cubic-anvil Riken-Seiki high-pressure apparatus at 4 GPa and 900 °C for 30 min. The temperature was slowly cooled before gradually releasing the pressure. This procedure resulted in around 50 mg of sample powder.

X-ray diffraction

The phase purity of samples was investigated by x-ray diffraction. The diffraction data were collected on a Panalytical X'pert Pro MPD diffractometer using Cu $K_{\alpha 1}$ radiation. The diffraction patterns were refined with the FULLPROF⁶ software suite. The quality of the data collected on the small $\text{Ba}_2\text{CuTeO}_6$ sample was not deemed sufficient for Rietveld analysis, and therefore Le Bail full profile fitting was performed instead. Rietveld refinement was used for Ba_2CuWO_6 . The crystal structures were visualized with VESTA.⁷

The measured x-ray diffraction patterns for $\text{Ba}_2\text{CuTeO}_6$ and Ba_2CuWO_6 are shown in Fig. 2. No impurity peaks are observed in $\text{Ba}_2\text{CuTeO}_6$ indicating that the material is phase pure. In the Ba_2CuWO_6 sample a minor (< 1%) BaWO_4 impurity is observed in addition to the main phase. The lattice parameters are in good agreement with literature.⁸

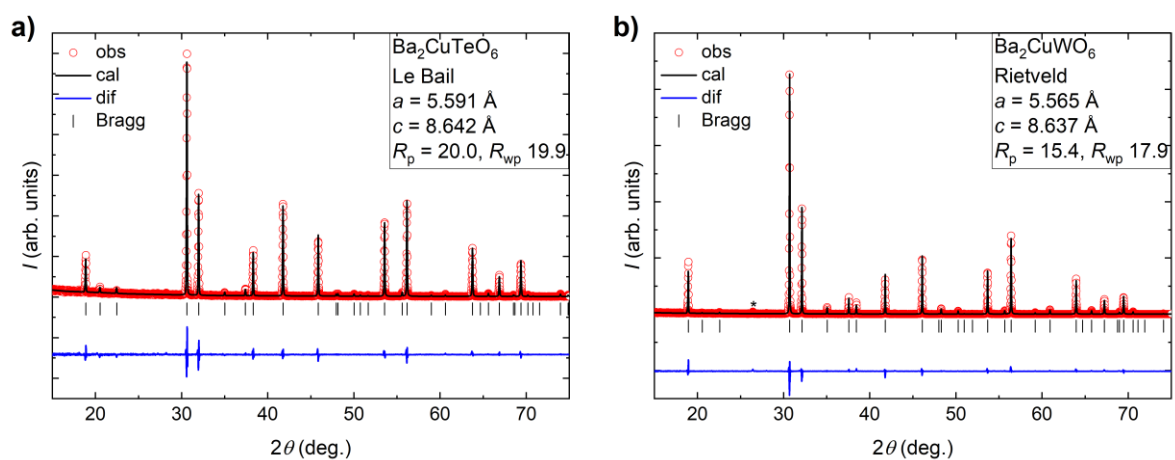


Fig. 2. X-ray diffraction patterns of (a) $\text{Ba}_2\text{CuTeO}_6$ and (b) Ba_2CuWO_6 . The minor BaWO_4 impurity in Ba_2CuWO_6 is marked with an asterisk. Bragg positions for the space group $I4/m$ are shown.

Magnetic measurements

Magnetic properties were measured with a Quantum Design MPMS3 SQUID magnetometer. 120 mg of Ba_2CuWO_6 and 25 mg of $\text{Ba}_2\text{CuTeO}_6$ were enclosed in gelatin capsules and placed in plastic straws for measurements. DC magnetic susceptibility was measured in the temperature range 2-400 K under an applied field of 1 T in zero-field cool (ZFC) and field cool (FC) modes.

References

- 1 <http://elk.sourceforge.net>.
- 2 J. P. Perdew, K. Burke and M. Ernzerhof, *Phys. Rev. Lett.*, 1996, **77**, 3865–3868.
- 3 S. Vasala, H. Saadaoui, E. Morenzoni, O. Chmaissem, T. Chan, J. Chen, Y. Hsu, H. Yamauchi and M. Karppinen, *Phys. Rev. B*, 2014, **89**, 134419.
- 4 H. C. Walker, O. Mustonen, S. Vasala, D. J. Voneshen, M. D. Le, D. T. Adroja and M. Karppinen, *Phys. Rev. B*, 2016, **94**, 064411.

- 5 A. I. Liechtenstein, V. I. Anisimov and J. Zaanen, *Phys. Rev. B*, 1995, **52**, R5467--R5470.
- 6 J. Rodríguez-Carvajal, *Phys. B*, 1993, 192, 55–69.
- 7 K. Momma and F. Izumi, *J. Appl. Crystallogr.*, 2011, **44**, 1272–1276.
- 8 D. Iwanaga, Y. Inaguma and M. Itoh, *J. Solid State Chem.*, 1999, **147**, 291–295.